An inflammation-induced mechanism for leukocyte transmigration across lymphatic vessel endothelium

Louise A. Johnson,[1] Steven Clasper,[1] Andrew P. Holt,[2] Patricia F. Lalor,[2] Dilair Baban,[3] and David G. Jackson[1]

[1]Medical Research Council (MRC) Human Immunology Unit, Weatherall Institute of Molecular Medicine, John Radcliffe Hospital, Headington, Oxford OX3 9DS, England, UK
[2]Liver Research Group, Institute of Biomedical Research, MRC Centre for Immune Regulation, University of Birmingham Medical School, Edgbaston, Birmingham B15 2TT, England, UK
[3]MRC Functional Genetics Unit, Department of Human Anatomy and Genetics, University of Oxford, Oxford OX1 3QX, England, UK

The exit of antigen-presenting cells and lymphocytes from inflamed skin to afferent lymph is vital for the initiation and maintenance of dermal immune responses. How such an exit is achieved and how cells transmigrate the distinct endothelium of lymphatic vessels are unknown. We show that inflammatory cytokines trigger activation of dermal lymphatic endothelial cells (LECs), leading to expression of the key leukocyte adhesion receptors intercellular adhesion molecule 1 (ICAM-1), vascular cell adhesion molecule 1 (VCAM-1), and E-selectin, as well as a discrete panel of chemokines and other potential regulators of leukocyte transmigration. Furthermore, we show that both ICAM-1 and VCAM-1 are induced in the dermal lymphatic vessels of mice exposed to skin contact hypersensitivity where they mediate lymph node trafficking of dendritic cells (DCs) via afferent lymphatics. Lastly, we show that tumor necrosis factor α stimulates both DC adhesion and transmigration of dermal LEC monolayers in vitro and that the process is efficiently inhibited by ICAM-1 and VCAM-1 adhesion-blocking monoclonal antibodies. These results reveal a CAM-mediated mechanism for recruiting leukocytes to the lymph nodes in inflammation and highlight the process of lymphatic transmigration as a potential new target for antiinflammatory therapy.

CORRESPONDENCE
David G. Jackson:
djackson@hammer.imm.ox.ac.uk

Abbreviations used: CAM, cell adhesion molecule; CCL, CC chemokine ligand; CCR, CC chemokine receptor; CMFDA, 5-chloromethylfluorescein diacetate; CXCL, CXC chemokine ligand; ENA-78, epithelial neutrophil activator 78; GRO, growth-regulated oncogene β; HDLEC, human dermal LEC; ICAM, intercellular adhesion molecule; JAM, junctional adhesion molecule; LEC, lymphatic endothelial cell; LYVE-1, lymph vessel endothelial hyaluronan receptor 1; MCP-1, monocyte chemoattractant protein 1; MDDC, monocyte-derived DC; MDLEC, mouse dermal LEC; MIP-3α, macrophage inflammatory protein 3α; RANTES, regulated on activation, normal T cell expressed and secreted.

The hallmarks of skin inflammation are an infiltration of the dermis by monocytes and activated T cells and an increase in draining lymph node cellularity primed by the large-scale immigration of dermal DCs via afferent lymphatics. These events are coordinated by cytokines, including TNF-α and IL-1, that induce maturation and emigration of skin-derived DCs (1), leading to exacerbation of inflammation or eventual fibrosis through pleiotropic effects within affected dermis. To date, much research has focused on the mechanisms by which T cells are recruited to inflamed tissues by transmigration of blood vessels (for review see 2). However, the equally important question of how DCs and other leukocytes are recruited to lymph nodes by transmigration of lymphatic vessels has received far less attention (3).

Knowledge about the mechanisms for the entry of DCs into lymphatics is mostly restricted to chemotaxis and the effects of chemokines on the process. For example, CC chemokine receptor 7 (CCR7), which binds the lymph node/lymphatic endothelial–derived CC chemokine ligand 21 (CCL21) and CCL19, is expressed in mature DCs and mediates their trafficking from tissue to lymph nodes (4–6). Recent evidence indicates the same receptor also mediates exit of $CD4^+$ effector memory T cells from tissue to lymph (7, 8). Moreover, deletion of the gene for CCR7 in knockout mice abolishes migration of Langerhans cells into dermal lymphatics, whereas the absence of lymph node CCL21 (as in the *plt* mouse, paucity of lymph node T cells) suppresses recruitment of DCs to draining lymph nodes and subsequent T cell–mediated immunity (9, 10). Nonetheless, it remains unclear whether these

The online version of this article contains supplemental material.

The Journal of Experimental Medicine

important lymphatic trafficking events are regulated solely by chemokines or whether there is an additional requirement for adhesion between leukocytes and lymphatic endothelium in the process.

In the case of the blood vasculature, it is well documented that adhesion and migration across inflamed vessel endothelium typically involves cytokine-induced expression of key leukocyte–endothelial cell adhesion molecules (CAMs)—intercellular adhesion molecule 1 (ICAM-1), vascular CAM (VCAM-1), and E-selectin (in endothelium)—that promote adherence and diapedesis of lymphocytes and monocytes through ligation of the counterreceptors αLβ2/αMβ2 integrin (CD11a/CD18, CD11b/CD18, and LFA-1/Mac I) and α4β1 integrin (very late antigen 4) Sialyl Lewis^X-modified mucoproteins, respectively (for review see 11; 12–14). In contrast, cytokine-induced expression of these and other leukocyte–endothelial CAMs on lymphatic vessels has not been adequately explored, despite indications that ICAM-1 knockout mice have defects in lymph node recruitment of DCs (12, 13) and that expression of VCAM-1 in medullary sinus coincides with lymphocyte retention in inflamed lymph nodes (14).

The cellular route by which leukocytes transmigrate lymphatic endothelium is equally uncertain. The ultrastructure of lymphatic capillaries is distinct from that of small blood vessels; most notably, they are not invested with mural cells and do not have a conventional basement membrane (3, 15, 16). Moreover, the initial lymphatics culminate in blind-ended termini that display occasional interendothelial gaps (17, 18) through which plasma and dissolved macromolecules are drawn in response to the negative pressure evoked by the innate pumping activity of larger lymphatic collectors (19). Whether these gaps can also serve as entry points for leukocytes or whether entry involves transmigration at interendothelial tight junctions (paracellular route) or across the endothelial cell body (transcellular route) as in the blood vasculature (20, 21) is open to conjecture. Likewise, which, if any, of these routes contributes to the acceleration in leukocyte transmigration that is triggered by inflammation or how accelerated entry might be regulated is unclear. In the few cases where transmigration has been observed in detail (e.g., the entry of DCs to lymph vessels in inflamed mouse skin explants), leukocytes were seen to undergo massive shape changes during passage into the vessel lumen (22, 23). Thus, whatever the route of entry, it is likely that intimate contacts form between leukocytes and inflamed lymphatic endothelium that could well regulate cell transit.

We have focused on the molecular mechanisms of lymphatic transmigration in the belief that an understanding of the process is important not only from the standpoint of fundamental biology but also for the development of more effective therapies to block inflammation and enhance vaccine delivery. We have found that lymphatic endothelium undergoes a program of activation during inflammation to support increased leukocyte transmigration in which the adhesion molecules ICAM-1 and VCAM-1 play key roles.

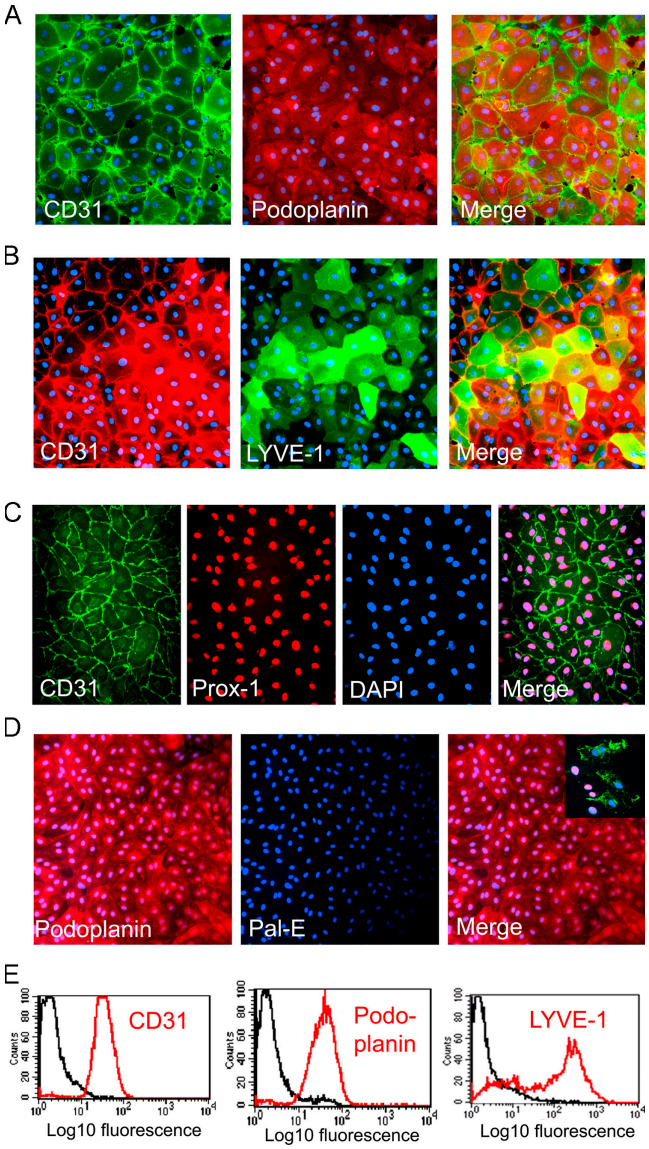

Figure 1. Characteristics of primary HDLECs isolated by LYVE-1 immunoselection. HDLECs isolated from human dermis by LYVE-1 immunomagnetic bead selection are shown after dual immunofluorescence staining for lymphatic and blood vascular-specific markers. (A and B) Confluent monolayers stained for the panendothelial marker CD31 and the lymphatic endothelial markers podoplanin or LYVE-1, respectively. In contrast to podoplanin, which is expressed by all HDLECs, LYVE-1 shows considerable variation, reflecting the heterogeneity seen in normal tissue lymphatics (see Results). (C) Triple staining for CD31, the lymphatic endothelial transcription factor PROX-1, and the nuclear stain DAPI. Note that all cells contain PROX-1–positive nuclei. (D) HDLEC monolayers stained for podoplanin and the blood vascular marker pal-E. Note the complete absence of pal-E–positive cells. Blood vascular endothelial cells positive for pal-E in the mixed endothelial culture preceding LYVE-1 immunoselection are shown for comparison (inset). (E) FACS histograms of HDLECs stained for CD31, podoplanin, or LYVE-1 (red). Isotype-matched controls are shown (black).

These important findings reveal a functional similarity between two otherwise distinct vasculatures and point to a much more active role for the lymphatics in inflammation than previously anticipated.

RESULTS

Cytokine-induced expression of key leukocyte adhesion molecules and chemokines in primary human dermal lymphatic endothelial cells (HDLECs)

To generate cells for analysis of the inflammatory response and its effects on DC transmigration, we isolated primary HDLECs from the dermis of freshly resected breast tissue or abdominoplasty by enzymatic digestion and magnetic bead immunoselection using antibody to lymph vessel endothelial hyaluronan receptor 1 (LYVE-1), a molecule whose preferential expression in lymphatic endothelium has been well documented (see Materials and methods) (24–26). The resulting cells comprised at least 99% LECs, as assessed by immunostaining for the sialomucin marker podoplanin (27) and the lymphatic lineage-associated transcription factor Prox-1 (28, 29), either alone or in combination with the panendothelial marker CD31 (Fig. 1, A, C, and E) (30). Parallel immunostaining for LYVE-1 (both alone and in combination with CD31) showed that the majority of the population was positive for the receptor even though there was clear heterogeneity in the level of expression among individual LECs (Fig. 1, B and E). This is in line with the observations of other researchers that indicate the receptor is expressed to variable extents in individual lymphatic vessels (19, 31) and primary LEC lines (32, 33, 34, 35), as well as with our own findings that LYVE-1 can be specifically downmodulated in cultured LECs, e.g., after exposure to cytokines

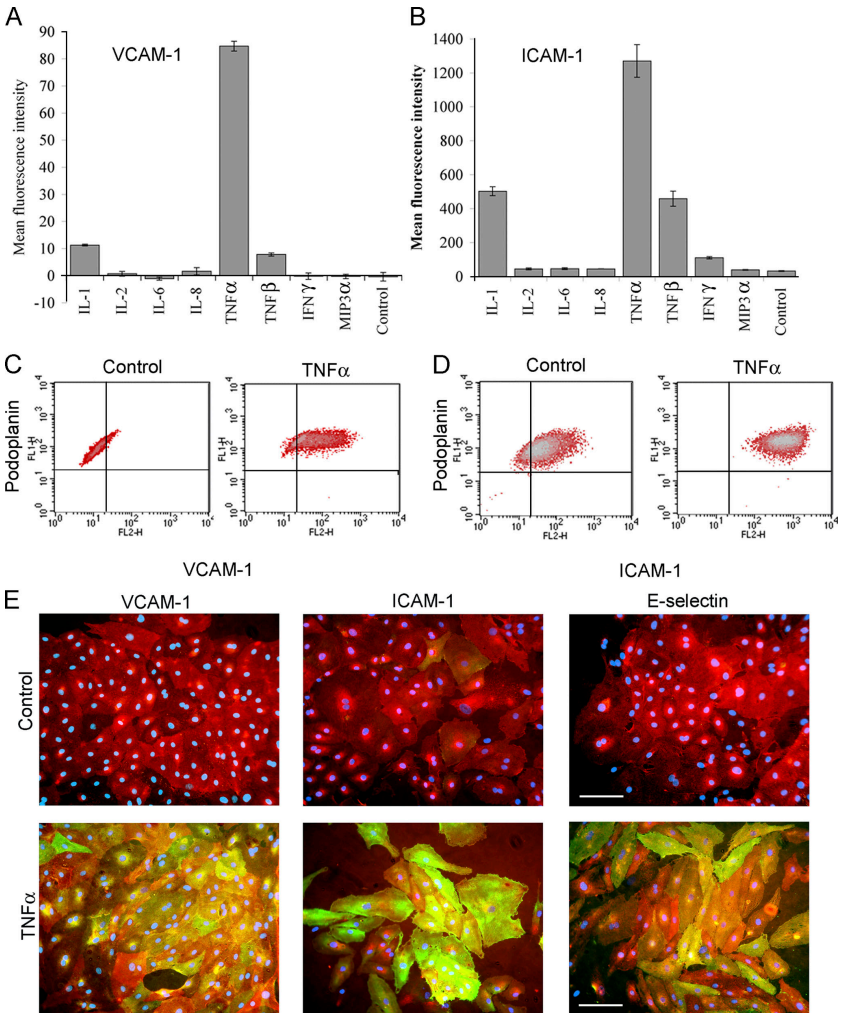

Figure 2. Inflammatory cytokines up-regulate surface expression of ICAM-1, VCAM-1, and E-selectin in cultured HDLECs. Cells were cultured for 24 h in the presence of individual proinflammatory cytokines or chemokines before immunostaining for either (A) VCAM-1 or (B) ICAM-1 and quantitation by FACS analysis. Data represent the mean ± SEM ($n = 3$). (C and D) Dot plots show VCAM-1 or ICAM-1 expression in HDLECs cultured in the presence or absence (control) of TNF-α and assessed by dual staining for podoplanin and CAMs. Note that all cells expressing CAMs are positive for podoplanin (top right quadrants). (E) Representative double immunofluorescence micrographs showing induction of CAMs and E-selectin (green) in podoplanin-positive (red) HDLECs, as indicated with nuclei counterstained for DAPI. Bar, 50 μm.

(Fig. S1 E, available at http://www.jem.org/cgi/content/full/jem.20051759/DC1; see Fig. S3 B; and not depicted). Importantly, no cells expressing the blood vascular endothelial-specific, vesicle-associated pal-E antigen (36, 37) were detected in our LEC cultures, these having been efficiently depleted in two successive rounds of LYVE-1 immunoselection (Fig. 1 D).

We next investigated the effects of inflammatory cytokines, focusing in particular on the leukocyte adhesion molecules ICAM-1, VCAM-1, and E-selectin, whose surface expression is known to be induced on activated blood vascular endothelium (38–40). As shown by FACS analysis and immunofluorescence microscopy (Fig. 2, A–E), a minor proportion of resting HDLECs expressed low levels of ICAM-1, whereas VCAM-1 and E-selectin were virtually absent. However, treatment with the cytokine TNF-α led to a dramatic up-regulation in surface expression (40–80-fold) of all three CAMs. These effects of TNF-α were both potent (requiring levels below 1 ng/ml for half-maximal induction; Fig. S1**)** and rapid ($T_{1/2}$ of 6–12 h for ICAM-1 and VCAM-1; $T_{1/2}$ of ∼4 h for E-selectin; Fig. 3, A–C). The characteristics of the response, its magnitude, and the transient nature of E-selectin expression (Fig. 3 C) were rather similar to those previously described for blood vascular endothelium (i.e., the human umbilical vein epithelial cell line; references 41, 42). Moreover, the induction of CAM expression by TNF-α appeared to be independent of mitogenesis or apoptosis within the range used in our experiments, involved no loss of cell integrity, and was completely reversible within 24 h of cytokine withdrawal (Fig. S2, A–C, available at http://www.jem.org/cgi/content/full/jem.20051759/DC1). Among other cytokines, TNF-β (lymphotoxin-α), IL-1α, and to a marginal extent IFN-γ also induced expression of ICAM-1, whereas IL-2, IL-6, IL-8, and the inflammatory chemokine macrophage inflammatory protein 3α (MIP-3α; CCL20) had no such effect (Fig. 2, A and B).

As induction of CAMs had not been reported previously in LECs, we considered the possibility that the CAM-positive cells in our experiments represented a subpopulation of contaminating blood vascular endothelial cells. However, two-color flow cytometry and immunofluorescence microscopy (Fig. 2, C–E**)** clearly demonstrated that all VCAM-1– and

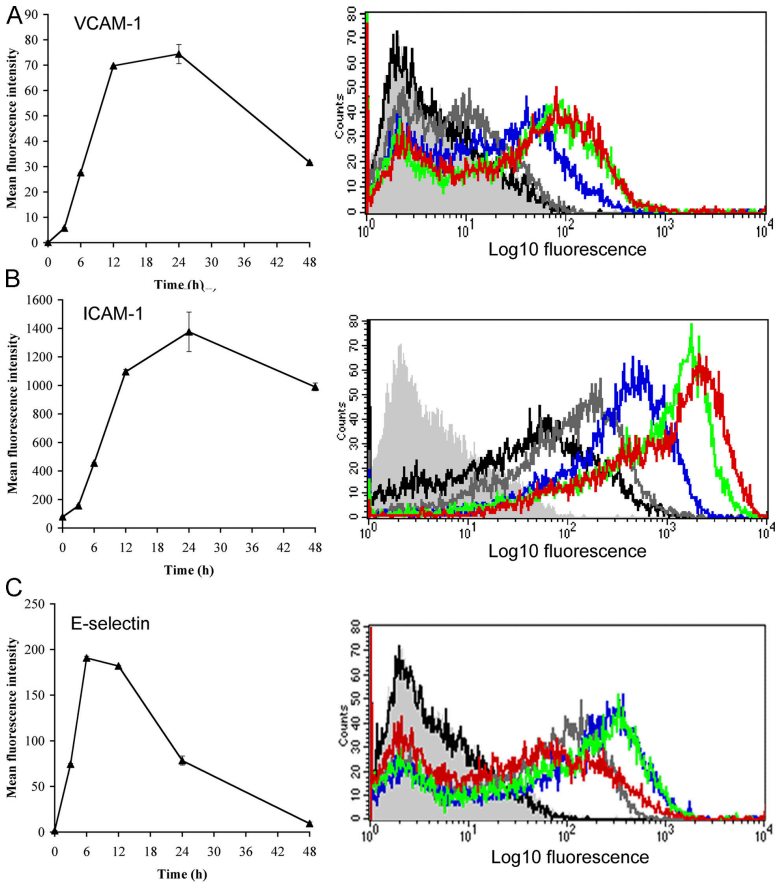

Figure 3. Kinetics of TNF-induced CAM and E-selectin expression in cultured primary HDLECs. (A–C) Respective time courses for induction of VCAM-1, ICAM-1, and E-selectin in HDLECs cultured for 0–48 h in the presence or absence of 1 ng/ml TNF-α, as assessed by FACS analysis. Representative histograms are shown for cells stained with isotype-matched control Ig (light gray) or mAbs to the appropriate adhesion molecules in unstimulated cells (black) or cells treated with TNF-α for 3 h (dark gray), 6 h (blue), 12 h (green), and 24 h (red).

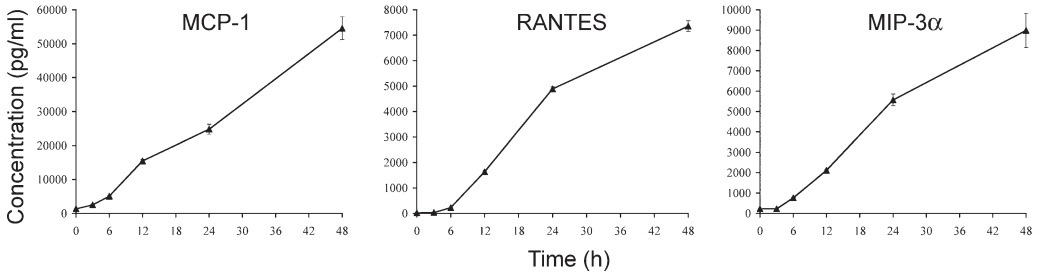

Figure 4. TNF-α induces proinflammatory chemokine production in cultured primary HDLECs. Cells were stimulated with 1 ng/ml TNF-α over a time course of 48 h, and concentrations of MCP-1, RANTES, and MIP-3α secreted into the culture supernatant were measured by ELISA. Data represent the mean ± SEM ($n = 3$).

ICAM-1–expressing cells were positive for podoplanin, thus confirming their identity as LECs. Moreover, we consistently observed induction of CAMs in a total of five independent cell preparations isolated by the LYVE-1 immunoselection procedure, in addition to preparations of HDLECs immunoisolated by either CD34/podoplanin selection (43) or outgrowth from commercial human dermal microvascular cell cultures (35) and in mouse dermal LECs (MDLECs) immunoisolated by LYVE-1 selection (Fig. S3, available at http://www.jem.org/cgi/content/full/jem.20051759/DC1; and not depicted). Thus, we are confident that the capacity to express leukocyte CAMs is a genuine property of the bulk HDLEC population rather than the result of contamination with biliary epithelial cells or a subpopulation undergoing dedifferentiation.

Finally, we investigated the effects of TNF-α on the production of leukocyte chemokines using appropriate ELISAs. The results (Fig. 4) show that resting, unstimulated HDLEC cultures secrete only trace levels of the major T cell and monocyte chemokines regulated on activation, normal T cell expressed and secreted (RANTES; CCL5), monocyte chemoattractant protein 1 (MCP-1; CCL2), and (MIP-3α; CCL20), confirming and extending upon previous findings (43). Importantly, however, stimulation with TNF-α triggered a considerable (>100-fold) rise in secretion of all three chemokines over a period of 24–48 h, reaching final levels of 7–55 ng/ml (Fig. 4). In contrast, secretion of both Epstein-Barr virus–induced molecule 1 ligand chemokine (CCL19) and secondary lymphoid tissue (CCL21)—chemokines associated with lymph node trafficking (4)—was below detectable levels (80 and 15 pg/ml, respectively; unpublished data) and was evidently not induced by treatment of LECs with inflammatory cytokines.

Extent of the inflammatory cytokine–induced expression program in LECs revealed by microarray analysis

To define inflammation-induced changes in HDLEC gene expression more comprehensively, we examined the RNA profiles of control and TNF-α–treated cells by gene chip array analysis using Affymetrix human U-133 arrays. The results (summarized in Table I and completely presented in Table S1, available at http://www.jem.org/cgi/content/full/jem.20051759/DC1) revealed a total of 424 genes that were up-regulated and 171 that were down-regulated by a factor of twofold or greater ($P \leq 0.1$). Notably, VCAM-1 (214-fold), ICAM-1 (7.7-fold), and E-selectin (160-fold) were all highly up-regulated, as were the levels of the leukocyte chemokines MCP-1, RANTES, and MIP-3α, confirming our findings at the protein level using FACS analysis and ELISA (see previous section). Moreover, RNA levels were also up-regulated for the neutrophil chemoattractants epithelial neutrophil activator 78 (ENA-78; CXC chemokine ligand 5 [CXCL5]) and growth-regulated oncogene β (GROβ; CXCL2), the monocyte/macrophage chemokines fractalkine (CX_3CL1) and CSF-1, and CCR10, a receptor for the chemokine CCL27 (cutaneous T cell–attracting chemokine)

Table I. Up-regulation of representative genes

Transcript	Fold change ($P < 0.05$)
VCAM-1	214
ICAM-1	7.7
E-selectin	160
Claudin-1	6.7
MIP-3α (CCL20)	444
ENA-78 (CXCL5)	388
RANTES (CCL5)	48
GROβ (CXCL2)	38
Fractalkine (CX_3CL1)	18.3
IL-6	18
MCP-1 (CCL2)*	7
IL-32*	5.8
CSF-1	3.7
CCR10	7
IL-12R*	2.4
Toll-like receptor 2	26
Toll-like receptor 1	3.1
MMP19	3.6
ADAMTS3	7.4
TNFSF9 (CD137)	35
TNFSF3 (LT-β)	23

Representative genes were up-regulated more than twofold by TNF-α stimulation of primary HDLECs at $P < 0.05$ (or $P < 0.1$, as indicated by *).

produced by inflamed epidermal keratinocytes (44), indicating a broad chemoattractant response within inflamed lymphatic endothelium. Interestingly, the array data also showed significant up-regulation of Toll-like receptor 2, the tight junctional component claudin-1, and the metalloproteinases MMP19 and ADAMTS3 (Table I). However, there was no change in abundance of transcripts for either CCL21 or CCL19, both of which are implicated in the exit of DCs from tissues to afferent lymphatics and trafficking to lymph nodes (9, 10).

Comparable changes in the transcriptional profile of MDLECs were induced by treatment with TNF-α, as revealed in microarray analyses using the Affymetrix mouse 430 array (Table S2, available at http://www.jem.org/cgi/content/full/jem.20051759/DC1), indicating the broad similarity in LEC response to inflammation between species.

In vivo evidence of a functional role for VCAM-1 and ICAM-1 in inflammation-induced lymphatic transmigration

Having established inflammation-induced expression of leukocyte CAMs in primary LECs in vitro, we next asked whether a similar response occurs during inflammation in vivo, using the well-characterized oxazolone-induced skin contact hypersensitivity model in BALB/c mice (45, 46). To achieve this, we prepared sections of dermis from inflamed and contralateral uninflamed ears (see Materials and methods) at various time points after oxazolone challenge and immunostained for CAMs in both whole-mount and thin sections. The results (Fig. 5, A and B) show that VCAM-1 and ICAM-1 are indeed expressed on inflamed lymphatic vessels—distinguished by their expression of podoplanin and comparatively large vessel diameters—in addition to small blood capillaries, whereas both CAMs were absent from the lymphatics of unchallenged tissue. Interestingly, expression in inflamed lymphatics was more focal than in inflamed blood vessels (Fig. 5, A and B; and not depicted), possibly indicative of different kinetics of induction within the two vasculatures. Nevertheless, quantitative estimates revealed that ∼50% of podoplanin-positive lymphatics stained for ICAM-1 and 60% for VCAM-1 within 18–24 h of allergen administration (Fig. 5, C and D). Similar levels of CAM expression were also seen among podoplanin-positive lymphatics (60% ICAM-1$^+$ vessels vs. 70% VCAM-1$^+$ vessels) 24 h after direct stimulation with TNF-α when ex vivo mouse skin explants were incubated with the cytokine (unpublished data). Moreover, visualization of APCs in the dermis of oxazolone-treated mice by immunostaining for MHC class II, ICAM-1, and podoplanin revealed many such cells in close association with CAM-positive lymphatic vessels (Fig. S4, available at http://www.jem.org/cgi/content/full/jem.20051759/DC1), suggesting but not proving that ICAM-1 might indeed play a role in lymphatic transmigration in an inflammatory context. The diameter of these superficial vessels (average ∼50 μm) is also consistent with their identity as initial lymphatics rather than the larger smooth muscle–invested lymphatic collectors (100–200 μm) that are found in the deeper dermis.

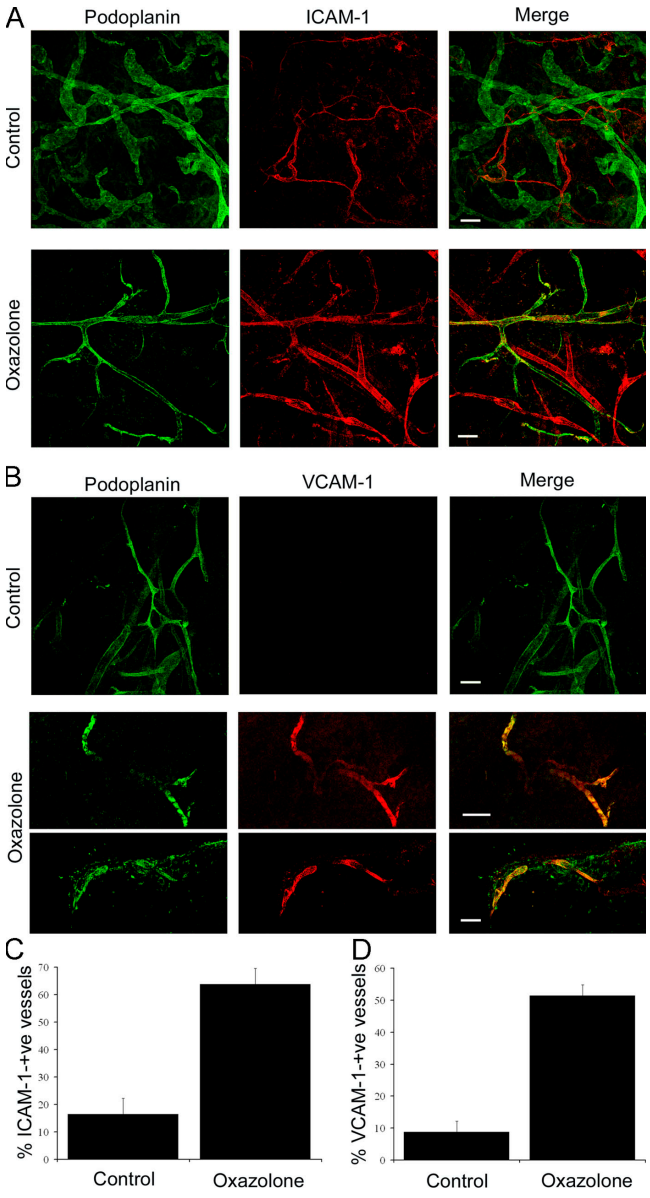

Figure 5. In vivo expression of ICAM-1 and VCAM-1 in mouse dermal lymphatics induced by skin contact hypersensitivity. Skin inflammation was induced in mouse ear by sensitization and subsequent challenge with oxazolone before analysis of lymphatic vessel CAM expression by immunofluorescence microscopy. (A and B) Whole-mount sections of oxazolone-challenged and contralateral-unchallenged (control) ears dual-stained for podoplanin (green) and ICAM-1 or VCAM-1, respectively (red). Note the weak expression of ICAM-1 confined to podoplanin-negative (blood) vessels in uninflamed skin (A) and the focal up-regulation of both ICAM-1 and VCAM-1 on podoplanin-positive (lymphatic) vessels in inflamed skin (A and B). Images were captured by confocal microscopy. Bars, 100 μm. (C and D) Quantitative estimates for the numbers of ICAM-1$^+$/podoplanin$^+$ and VCAM-1$^+$/podoplanin$^+$ vessels determined by counting 21 separate fields of view (7 fields/mouse) in control and oxazolone-treated ear sections. Data represent the mean ± SEM.

To assess the functional role of CAMs in lymphatic transmigration in vivo, we imposed blockade by the injection of oxazolone-treated mice with neutralizing antibodies to ICAM-1 (mAb YN1/1.7.4 [47]) or VCAM-1 (mAb 6C7.1 [48]) and tracked migration of cutaneous DCs to lymph nodes detected by FITC skin painting. The results of these experiments (Fig. 6 A) show that blocking antibodies to either VCAM-1 or ICAM-1 consistently suppressed lymph node trafficking of $FITC^+/CD11c^+$ by >60% compared with isotype-matched Ig controls. Given that cutaneous DCs migrate to lymph nodes almost exclusively via afferent lymphatics rather than entering the blood circulation (49), these findings argue for a role of ICAM-1 and VCAM-1 in either proximal vessel entry, migration, or egress from the draining lymph node. To further distinguish between these possibilities, we traced the fate of emigrating DCs during CAM adhesion blockade in a separate set of experiments in which we adoptively transferred mature 5-chloromethylfluorescein diacetate (CMFDA)–labeled bone marrow–derived DCs into the dermis of oxazolone-treated mice. As shown in Fig. 6 B, virtually all CMFDA-labeled DCs had already exited the dermis by 24 h after adoptive transfer in mice treated with isotype-matched control Ig and few, if any, were detected in the vicinity of lymphatics. In contrast, large numbers of CMFDA-labeled DCs could be seen in the dermis of ICAM-1 mAb YN1-1–treated mice, and these were associated

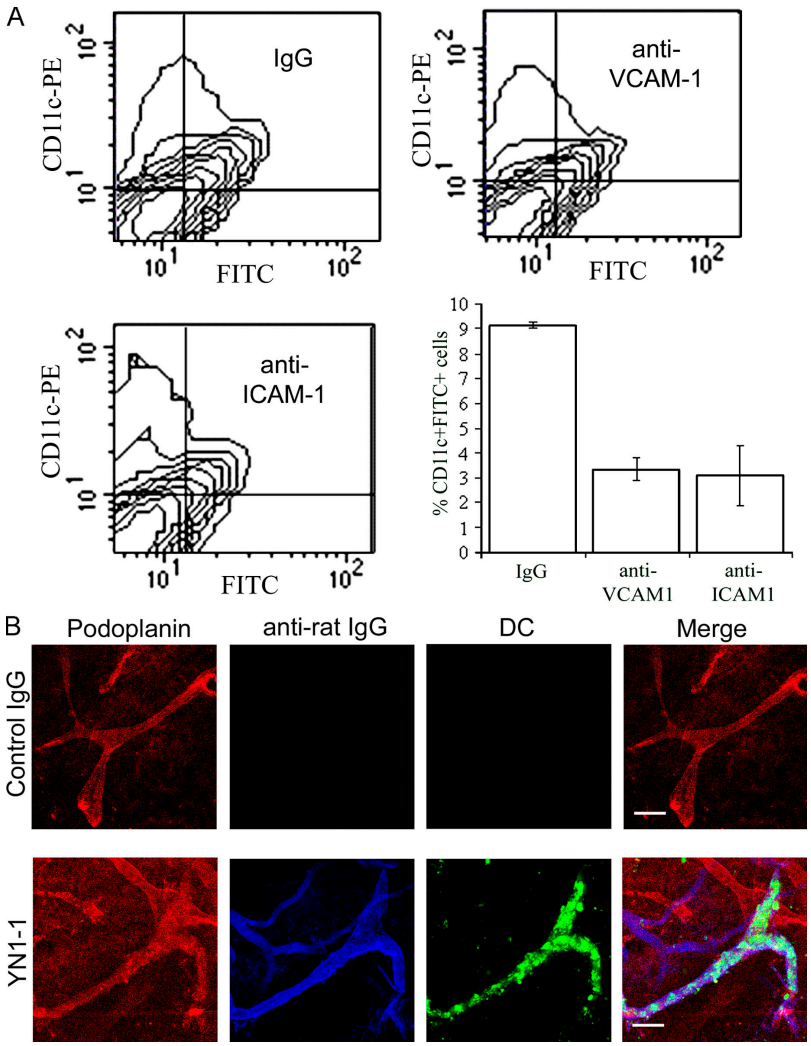

Figure 6. In vivo trafficking of skin DCs via afferent lymphatics is dependent on ICAM-1 and VCAM-1 adhesion. The involvement of ICAM-1 and VCAM-1 in the trafficking of DCs via afferent lymphatics was investigated in mice with oxazolone-induced skin hypersensitivity. (A) Recoveries of $FITC^+/CD11c^+$ skin DCs in the draining lymph nodes 24 h after FITC skin painting of oxazolone-sensitized mice that received prior injection of neutralizing mAbs to VCAM-1, ICAM-1, or control rat Ig. Data represent the mean recoveries ± SEM (obtained from three separate experiments). (B) To show retention of DCs within the skin, CMFDA-labeled bone marrow–derived DCs from a littermate were intradermally injected into the ear tissue of sensitized mice that received prior injection of a neutralizing mAb to ICAM-1 (YN1-1) or control rat Ig. After 24 h, ears were removed, and whole-mount staining was performed using anti-podoplanin with Alexa Fluor 568 (red) and Cy5-conjugated goat anti-rat Cy5 (blue) to detect binding of neutralizing antibody within the tissue. Bars, 100 μm.

with podoplanin-positive initial lymphatics that could be seen to express high levels of ICAM-1 through YN1-1 staining (Fig. 6 B, bottom). There was no obvious association of DCs with ICAM-1-positive blood vessels. Although the ICAM-1 molecule is expressed at low levels by mature DCs themselves, this was previously shown not to be required for trafficking to lymph nodes (13). Hence, our results provide new evidence that CAMs expressed on lymphatic endothelium are required for efficient DC transmigration of inflamed lymphatics.

Analysis of the molecular mechanisms for ICAM-1– and VCAM-1–mediated translymphatic migration

Finally, we investigated the mechanistic basis for CAM-mediated lymphatic transmigration using a quantitative in vitro assay that measured the passage of in vitro LPS- stimulated $CD14^+$ human blood monocyte-derived DCs (MDDCs) across monolayers of primary HDLECs in Boyden chambers. The mature promigratory phenotype of these DCs ($CD80^+$, $CD83^+$, $CD86^+$, and MHC class II^{high}) is shown in Fig. S5 (available at http://www.jem.org/cgi/content/full/jem.20051759/DC1).

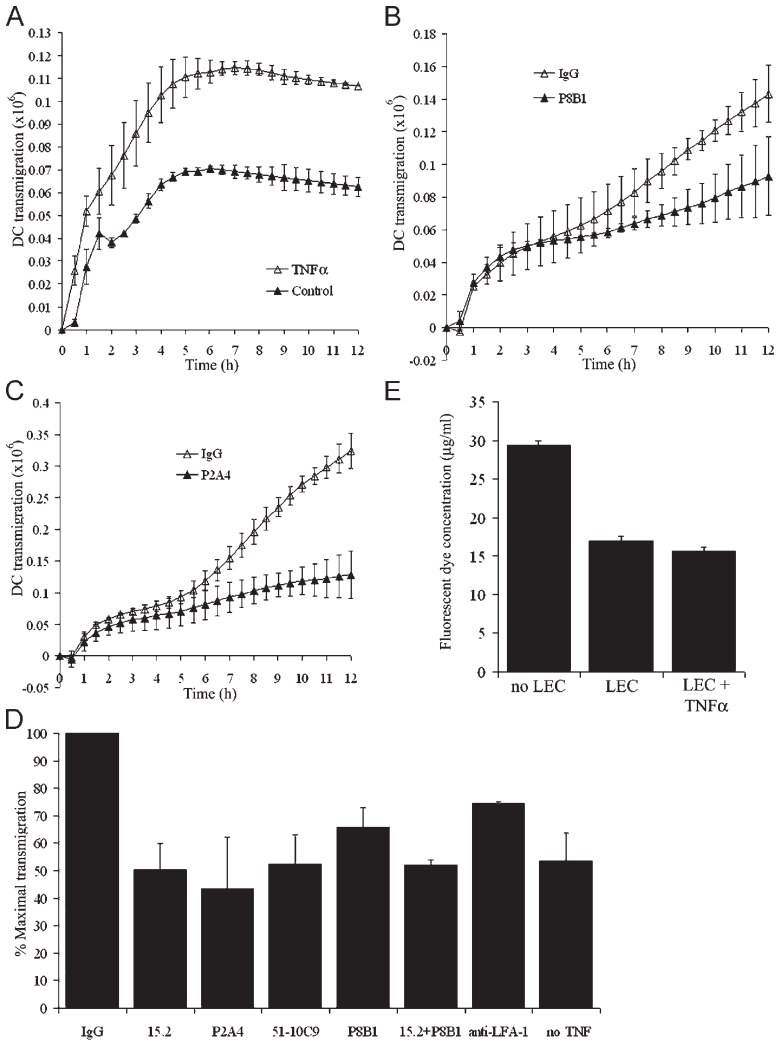

Figure 7. MDDC transmigration of TNF-α–stimulated HDLEC monolayers is dependent on ICAM-1 and VCAM-1. Transmigration of Cell Tracker Green fluorescently labeled MDDCs across either unstimulated or TNF-α–stimulated HDLEC monolayers plated on the undersurface of Fluoroblok filters was monitored in the presence or absence of selected adhesion blocking antibodies over a 12-h period. Progress curves are shown for MDDC transmigration across (A) control unstimulated versus TNF-α–stimulated HDLECs, (B) TNF-α–stimulated HDLECs treated with control rat IgG versus VCAM-1–neutralizing mAb P8B1, and (C) TNF-α–stimulated HDLECs treated with control rat IgG versus ICAM-1–neutralizing mAb P2A4. Data represent the mean ± SEM ($n = 4$). (D) Comparative effects of individual ICAM-1 mAbs 15.2 and P2A4, VCAM-1 mAbs 51-10C9 and P8B1, ICAM-1 mAb 15.2 and VCAM-1 mAb P8B1 together, the LFA-1 mAb 24, and control mouse IgG on MDDC transmigration of TNF-α–stimulated HDLECs. The level of transmigration across unstimulated HDLECs is shown for comparison. Data from three independent experiments are normalized to the measured levels of transmigration in the presence of control IgG (100% maximal transmigration) in each case and represent the mean ± SEM ($n = 4$). (E) Permeability of confluent HDLEC monolayers to unconjugated Alexa Fluor 488 measured as dye recovered in the lower chamber of Fluoroblok filter wells after a 6-h incubation at 37°C. Data represent the mean ± SEM.

To mimic the tissue exit of DCs via initial lymphatics in vivo (i.e., basolateral to luminal migration), we plated HDLECs on the lower side of UV-opaque Fluoroblok filters and monitored transit of CMFDA (Cell Tracker Green)-labeled MDDCs from the upper to the lower compartment. The resulting monolayers showed some permeability to a small-molecule probe (fluorescent-labeled goat IgG; see Materials and methods) even when fully confluent (Fig. 7, E and F; and Fig. S6), perhaps reflecting some retention of the native overlapping junction architecture. As shown by the time course in Fig. 7 A, LPS-matured DCs displayed substantial migration across resting unstimulated HDLECs (~10% of input cells transmigrated after 8 h). However, earlier stimulation of HDLEC monolayers with 1 ng/ml TNF-α for 24 h led to a substantial increase in the rate and extent of MDDC transmigration after a lag period of ~3 h (range = 1–3 h) after MDDC

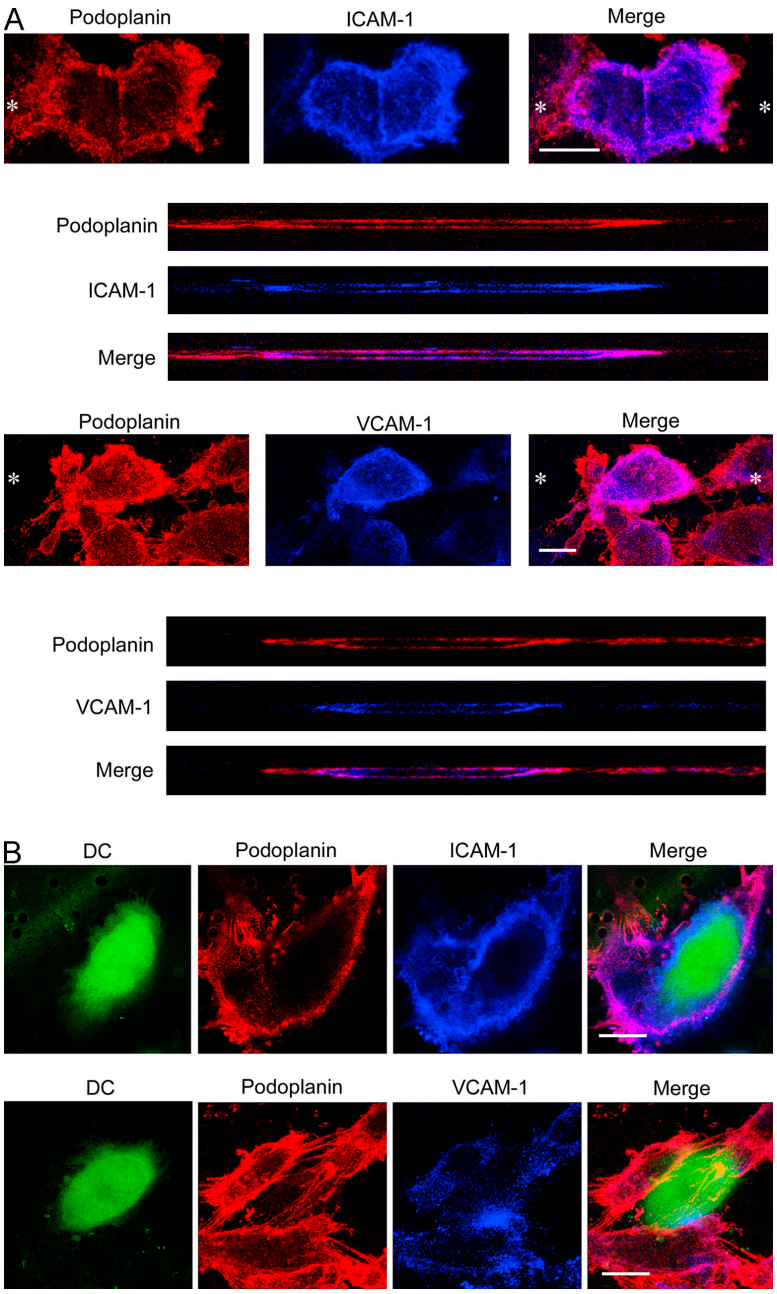

Figure 8. VCAM-1 and ICAM-1 are expressed on both luminal and basolateral surfaces of HDLECs. Cells were cultured on clear-membrane inserts and stimulated with TNF-α for 24 h before staining with antipodoplanin (red) and either anti–ICAM-1 or anti–VCAM-1 (blue) and analysis by confocal microscopy. Staining was performed either on HDLECs cultured (A) in the absence of MDDCs or (B) at 10 h after addition of Cell Tracker Green fluorescently labeled MDDCs. (A, top) Asterisks depict the axis through which individual LECs were imaged in z-section (bottom). Bars, 10 μm.

addition (Fig. 7 A). This TNF-α–induced component of transmigration was not caused by a simple increase in monolayer permeability because it was blocked in dose-dependent fashion by the addition of neutralizing antibodies specific to either ICAM-1 (mAbs P2A4 or 15.2) or VCAM-1 (mAb 51-10C9), added either singly or in combination (Fig. 7, B–D; and Fig. S7). No such inhibition was seen with unstimulated LECs (unpublished data). In addition to these CAM-blocking mAbs, considerable inhibition of transmigration was also observed after the addition of the β2 integrin–neutralizing antibody mAb 24, consistent with a role for this integrin as an LEC CAM counterreceptor on DCs (Fig. 7 D). However, in the case of the ICAM-1 mAbs, inhibition of transmigration could be assigned to the blockade of antigen on LECs rather than DCs (which express lower but substantial levels of ICAM-1; Fig. S5) because preincubation with the latter had no effect (not depicted).

Interestingly, MDDCs were also found to transmigrate TNF-α–activated LECs in the luminal to basolateral direction (assessed by plating LECs on the upper surface of filters) with a similar time course and CAM dependence to basolateral-luminal transmigration (Fig. S8, available at http://www.jem.org/cgi/content/full/jem.20051759/DC1; and not depicted). To determine whether these properties are reflected in the polarity of CAM distribution in TNF-activated LECs, we performed dual fluorescence staining of monolayers for ICAM/VCAM and podoplanin and analyzed the resulting sections by confocal microscopy. As shown in Fig. 8, both ICAM-1 and VCAM-1 could be seen on the apical as well as the basolateral face of the endothelial plasma membrane, indicating no obvious polarity in distribution. Moreover, ICAM-1 appeared to be distributed in a ring beneath individual MDDCs contacting the LEC monolayer as visualized by CMFDA labeling (Fig. 8 A), whereas VCAM-1 showed a more patchy distribution (Fig. 8 B).

The clearest interpretation of our findings is that ICAM-1 and VCAM-1 in LECs mediate a leukocyte adhesion step that is prerequisite for activation-induced transmigration, analogous to the CAM-mediated firm adhesion that precedes leukocyte diapedesis in blood vascular endothelium. To explore this issue further, we measured adhesion of CMFDA-labeled MDDCs to TNF-activated HDLECs cultured in 24-well plates. As shown in Fig. 9, MDDCs displayed considerable binding to activated LECs within 3 h of incubation, increasing twofold after 10 h in a time course that resembled MDDC transmigration (Fig. 7). Moreover, when the effects of antibody blockade were examined (ICAM-1 mAbs P2A4 and 15.2 and VCAM-1 mAbs Ig11 and P8B1), it was clear that only binding at the later (10 h) and not the earlier (3 h) time point was reduced (Fig. 9). Binding during this early lag period is therefore CAM-independent and may represent a period during which chemokine-induced activation of DC integrins occurs.

In summary, we conclude that MDDC transmigration of activated LECs in vitro involves an initial CAM-independent interaction between the two cell types that is followed by secondary ICAM/VCAM-mediated adhesion and transmigration.

DISCUSSION

The mechanisms by which leukocytes exit the tissues via lymph and migrate to draining lymph nodes have remained unclear despite their central importance for efficient generation of the immune response. The afferent lymphatics must cater for both low-level trafficking of APCs during normal immune surveillance and the increase in DC, effector memory T cell, and neutrophil trafficking that is triggered by tissue inflammation (for review see reference 3). In this manuscript, we set out to define the mechanisms underlying these processes using a combination of in vitro studies with primary dermal LECs and in vivo studies with a mouse model of oxazolone-induced skin inflammation. Specifically, we showed that cultured primary HDLECs and MDLECs respond to the cytokines TNF-α and TNF-β (lymphotoxin-α), and to a lesser extent IL-1, by rapidly and reversibly upregulating expression of the leukocyte adhesion molecules ICAM-1, VCAM-1, and E-selectin, together with synthesis and release of chemotactic agents, including the key inflammatory CC chemokines CCL5 (RANTES), CCL2 (MCP-1/JE), and CCL20 (MIP-3α). In addition, we demonstrated the induction of ICAM-1 and VCAM-1 expression in afferent lymphatic vessels draining the skin of oxazolone-treated mice in vivo and presented evidence that administration of

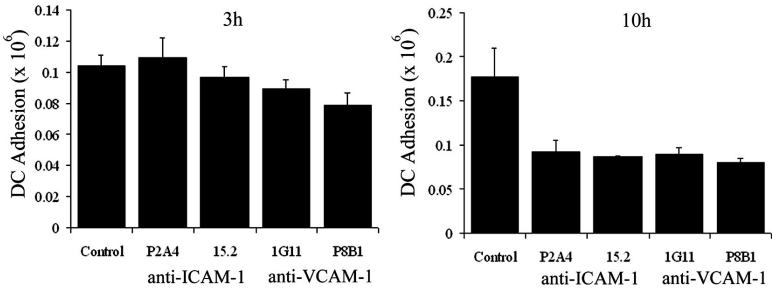

Figure 9. MDDC adhesion to TNF-α–stimulated HDLECs is dependent on ICAM-1 and VCAM-1. Cell Tracker Green fluorescently labeled MDDCs were applied to TNF-α–stimulated HDLEC monolayers plated in 24-well plates, preincubated with either IgG control or ICAM-1 mAbs (15.2 or P2A4) or VCAM-1 mAbs (P8B1 or IGII), in triplicate. At 3 and 10 h, the numbers of adherent MDDCs were measured. Representative data from three independent experiments are shown and represent the mean ± SEM ($n = 3$).

ICAM-1– and VCAM-1–neutralizing antibodies blocked exit of CD11c-positive skin DCs via afferent lymphatics. Finally, we presented evidence from in vitro lymphatic transmigration assays with MDDCs that ICAM-1 and VCAM-1 mediate inflammation-induced transmigration by promoting leukocyte-endothelial adhesion.

The induction of CAM expression in activated lymphatic vessel endothelium reveals an unexpected similarity with the blood vasculature, where up-regulation of these same molecules in inflamed postcapillary venules promotes leukocyte transmigration by mediating firm adhesion (for review see reference 2). In hemovascular transmigration, ICAM-1 and VCAM-1 promote stable adhesion of leukocytes to the apical endothelial membrane surface after their initial capture from blood flow and tethering on E- and P-selectin (50). Binding via ICAM-1 and VCAM-1 then allows the adherent leukocytes to crawl toward intercellular junctions (51), where additional interactions with the homophilic adhesion molecules CD31 (platelet/endothelial cell adhesion molecule 1) and CD99, together with junctional molecules such as junctional adhesion molecule 1 (JAM-1) and VE-cadherin, promote diapedesis (52–54). The prediction from our own experiments that ICAM-1 and VCAM-1 would mediate lymphatic vascular transmigration through a similar mechanism of leukocyte adhesion was confirmed by our finding that LPS-treated MDDCs bind to TNF-activated LECs in static assays and that the interaction was blocked by CAM-neutralizing mAbs using similar concentrations to those that blocked transmigration. There is also the likelihood that events downstream of this CAM-mediated adhesion might be similar to those in the hemovasculature, given that primary HDLECs express similar junctional molecules, including VE-cadherin and JAMs, and that LEC monolayers can form both tight and adherens junctions in vitro (43). Furthermore, mice with targeted deletion of the gene for *JAM-1* (*JAM-A*) display abnormalities in DC trafficking to lymph nodes, consistent with a role for the molecule in lymphatic vessel diapedesis (55). Detailed functional studies of these molecules in lymphatics are therefore clearly warranted.

A key question regarding entry of leukocytes to the afferent lymphatics is whether transmigration occurs at the distinctive overlapping junctions found within some initial lymphatics, at conventional interendothelial junctions, or through the endothelial cell body. It is interesting to note that docking structures containing ICAM-1 and VCAM-1 that were shown to mediate leukocyte transcellular/paracellular migration in hemovascular endothelial cells have also been observed in cells resembling a lymphatic phenotype (56). Hence, it may be that leukocytes can transmigrate lymphatic endothelium using more than one mechanism, and it will be of major interest to determine the preferred route for individual leukocyte populations and the factors influencing such choice in future experiments.

It is generally assumed that most leukocyte traffic through afferent lymphatics involves transmigration in the basolateral to luminal direction. Nevertheless, it is also possible that reverse migration in a luminal to basolateral direction might occur. Such a notion is supported by our finding that ICAM-1 and VCAM-1 are expressed on both the upper and lower faces of the endothelial membrane in primary HDLECs in vitro and that activated HDLECs promote CAM-dependent migration of MDDCs equally in both directions. If this phenomenon occurs in vivo, it raises the intriguing possibility that some leukocytes might exit the afferent lymphatics and reenter at different points within inflamed tissue, a process that might increase the efficiency of immune surveillance. Bidirectional migration across activated lymphatic sinus endothelium could also be envisaged to play roles in trafficking within inflamed lymph nodes.

Finally, besides identifying mechanisms by which adhesion molecules facilitate transmigration of activated lymphatics, we also identified several chemokines that could potentially direct the process. Although existing evidence indicates that the major chemokine for directing lymphatic entry of mature DC and memory T cell entry is CCL21 (also known as secondary lymphoid chemokine, or *slc*), which binds the G protein–coupled receptor CCR7 (5, 9, 10), it seemed likely to us that other chemoattractants might also be involved. As indicated by the results of gene chip microarray analyses and chemokine ELISAs presented in this manuscript, it is now clear that activated HDLECs synthesize a large number of different chemoattractants, including the T cell/monocyte chemokines CCL20 (MIP-3α), CCL5 (RANTES), CCL2 (MCP-1), and CX_3CL1 (fractalkine). Release of these chemokines in vivo might be envisaged to promote lymph node trafficking of those newly extravasated monocytes and immature DCs bearing cognate CCR2, CCR5, CCR6, and CX3CR that enter skin and other tissues in response to inflammation and that subsequently mature into professional APCs (57, 58). Moreover, secretion into lymph could have long-range effects on cell trafficking in the blood vasculature (59). Thus, "activated" LECs may well be the source of CCL2 (MCP-1) in inflamed skin that was shown recently to be rapidly transported via afferent lymph to the luminal surface of draining lymph node high endothelial venues, where it triggered integrin-mediated arrest and recruitment of monocytes from the blood circulation (60). Overall, the broad range of chemoattractants that we observed in cytokine-stimulated LECs, including both monocyte/T cell chemokines and neutrophil chemokines such as CXCL2 (GROβ) and CXCL5 (ENA-78), suggests a far greater role for lymphatics in coordinating inflammatory leukocyte recruitment than has previously been appreciated.

In conclusion, we have shown for the first time that inflamed lymphatic endothelium promotes the exit of leukocytes from tissue to afferent lymph through newly induced expression of the adhesion molecules ICAM-1 and VCAM-1, which were previously thought to be specific for blood vessel transmigration. These findings reveal an overlap between the traffic signals within the blood and lymphatic circulations and identify the process of lymphatic transmigration as a potential target for antiinflammatory drug therapy.

MATERIALS AND METHODS

Human and animal studies. All studies using human tissue were approved by the Oxford Regional Ethics Committee. All animal studies were performed under the appropriate Home Office licenses and institute guidelines.

Isolation of primary HDLECs and MDLECs. HDLECs were prepared from healthy adults undergoing elective surgery (breast reduction and abdominoplasty). MDLECs were prepared from the skin of BALB/c pups. In both cases, skin was digested overnight at 4°C with 2 mg/ml Dispase (Invitrogen) in PBS, pH 7.5, to remove the epidermis. Dermal cells were released from human tissue by scraping, passed through a 70-μm cell strainer (BD Biosciences), and expanded in 0.1% gelatine-coated flasks in complete medium (EGM-2 MV; Cambrex Bio Science) at 37°C/5% CO_2 in a humidified atmosphere. Dermal cells were released from mouse skin by digestion for 30 min at 37°C with a mixture of 2 mg/ml collagenase A, 0.2 mg/ml ovine testicular hyaluronidase, 0.05 mg/ml DNase I, and 0.05 mg/ml elastase (all obtained from Roche). Digests were filtered through a 70-μm cell strainer, and cells were cultured overnight in complete EGM-2 MV medium. HDLECs and MDLECs were lifted with Accutase (PAA Laboratories) and immunoselected with mouse anti–human LYVE-1 mAb and rat anti–mouse LYVE-1 mAb, respectively, followed by magnetic retrieval with the appropriate MACS bead preparations (Miltenyi Biotec). The resulting cells were cultured in EGM-2 MV using plastic tissue culture flasks that had been precoated with 0.1% gelatin (Invitrogen). All experiments were performed on confluent cells.

Cytokines and chemokines. Recombinant cytokines and chemokines (R&D Systems) were used at the following concentrations: IL-1α, 1 ng/ml; IL-2, 2 ng/ml; IL-6, 20 ng/ml; IL-8, 50 ng/ml; TNF-α, 0.1–10 ng/ml (see Results); TNF-β, 100 ng/ml; IFN-γ, 100 ng/ml; and MIP3-α, 100 ng/ml. Recombinant mouse TNF-α was used at 100 ng/ml.

Antibodies. mAb to soluble mouse LYVE–1 Fc (25) was generated in the rat, and polyclonal antisera to mouse or human LYVE-1 were generated and used as described previously after purification of Ig using Protein A/G–Sepharose (25, 61). Other antibodies were rat anti–mouse CD31 (Cymbus Biotechnology); goat anti–mouse ICAM-1, SLC, and JE (R&D Systems); mouse anti–human ICAM-1 and ICAM-2 (Serotec); mouse anti–human E-selectin (R&D Systems); and mouse anti–human VCAM-1, CD31, and CD34 (BD Biosciences). Rabbit anti–human Prox-1 and anti–human podoplanin were purchased from Fitzgerald Industries International, Inc. Specificity of rabbit antisera was confirmed using podoplanin Fc. Hamster anti–mouse podoplanin (clone 8.1.1) was from the Developmental Studies Hybridoma Bank (University of Iowa, Iowa City, IA). Rabbit polyclonal sera against mouse and human podoplanin were donated by D. Kerjaschki (Medical University of Vienna, Vienna, Austria). Function-blocking mAbs P2A4 and P8B1 (anti–ICAM-1 and anti–VCAM-1, respectively) (62) were from the Developmental Studies Hybridoma Bank; 51-10C9 (anti–VCAM-1) was from BD Biosciences; and both 15.2 (anti–ICAM-1) and 24 (anti–LFA-1) were gifts from N. Hogg (Cancer Research UK London Research Institute, London, United Kingdom). Rat anti–mouse function-blocking mAbs against VCAM-1 (clone 6C7.1) (48) and ICAM-1 (YN1/1.7.4) (47) were gifts from D. Vestweber (University of Münster, Münster, Germany). Isotype-matched antibodies (mouse, rat, rabbit, and goat IgG) were purchased from Sigma-Aldrich. All other primary antibodies were obtained from Cancer Research UK. Secondary antibody Alexa Fluor 488 (green) or Alexa Fluor 568/594 (red) conjugates were obtained from Invitrogen.

Flow cytometry. Cells were lifted with Accutase (PAA Laboratories), suspended in incubation buffer (PBS–5% FCS, 0.1% azide) and incubated for 30 min at 5°C with primary antibody, followed by washing and reincubation for 30 min at 5°C with the appropriate Alexa Fluor 488 goat conjugate before analysis on a flow cytometer (FACSCalibur; BD Biosciences) using CellQuest software.

Immunofluorescent antibody staining of cells and tissues. For single/double immunofluorescent staining of cultured HDLECs and MDLECs in plastic dishes, appropriate primary antibodies were applied in PBS–5% FCS, and cells were incubated at 25°C for 30 min, followed by washing and reincubating with Alexa Fluor secondary antibodies in PBS–5% FCS. Samples were fixed in 2% formaldehyde-PBS (vol/vol) for 10 min and mounted in Vectashield-DAPI (Vector Laboratories) before viewing under a fluorescence microscope (Axiovert; Carl Zeiss MicroImaging, Inc.).

For whole-mount staining, tissues were fixed overnight at 5°C in paraformaldehyde (4% wt/vol in PBS, pH 7.4), blocked in PBS–Triton X-100 (0.3% vol/vol supplemented with dried milk, 3% wt/vol), and incubated with the appropriate primary antibodies overnight at 5°C and fluorescent-conjugated secondary antibodies for 2 h at 25°C before mounting in Vectashield and viewing on a confocal microscope (Radiance 2000; Bio-Rad Laboratories) with sequential scanning.

For preparation of thin frozen sections, tissues were frozen in OCT Embedding Medium (purchased from R.A Lamb Laboratory Supplies) before cutting 8-μm or thinner sections by cryostat. Primary antibodies were applied, followed by Alexa Fluor conjugates. Sections were mounted in Vectashield, and images captured using a confocal microscope with sequential scanning.

To visualize DC migration across HDLEC monolayers, primary HDLECs were seeded onto the underside of gelatin-coated clear cell culture inserts (3-μm pore size; BD Biosciences), as described for a transmigration assay (see MDDC-HDLEC transmigration assay). CMFDA-labeled MDDCs were applied, and after 10 h cells were fixed in paraformaldehyde and stained with rabbit antipodoplanin and mouse anti–VCAM-1 or anti–ICAM-1, and with goat anti–rabbit–conjugated Alexa Fluor 568 and goat anti–mouse Cy5 (Chemicon). Images were captured using a confocal microscope with xy and xz scanning.

Endothelial cell proliferation assay. The proliferation rate of HDLECs was determined using a colorimetric assay that measured reduction of MTT (3-(4,5-dimethylthiazol-2-yl)-2,5-diphenyl tetrazolium bromide) to the insoluble formazan product (63). In brief, 40 μl MTT solution (7.5 mg/ml in PBS, pH 7.5) was mixed with 200 μl culture medium and added to monolayers of endothelial cells cultured in 24-well dishes. After incubation for 1 h at 37°C, supernatants were discarded, and 200 μl of 0.04 M HCL in isopropanol was applied to the monolayer. Cell lysates were centrifuged for 4 min at 900 *g*, and the resulting supernatants were analyzed in a plate reader (model 680; Bio-Rad Laboratories) at 590 nm.

Chemokine ELISA. Supernatants from triplicate wells of confluent primary HDLECs and MDLECs were assayed for the chemokines RANTES, MCP-1 (JE), and MIP-3α using a commercial antigen capture ELISA method (Quantikine; R&D Systems), according to the manufacturer's instructions. In brief, appropriately diluted supernatants were applied in triplicate to precoated ELISA wells, alongside negative controls of medium alone and chemokine standards, applied in duplicate. Bound chemokines were detected using a secondary horseradish peroxidase–conjugated antibody and substrate for measurement in a microplate reader at 490 nm.

Oxazolone-induced contact hypersensitivity. BALB/c male mice aged 8–10 wk were sensitized by topical application of 3% (wt/vol) oxazolone (4-ethoxymethylene-2 phenyl-2-oxazoline-5-one; Sigma-Aldrich) in 95% aqueous. ethanol to the shaved abdomen (50 μl per mouse). The next day, a further 100 μl of 2.5% (wt/vol) oxazolone was applied to the same site. On day 5, the dorsal surface of the left ear was challenged in each case by topical application of 0.5% oxazolone solution (50 μl per ear), while the right ear (control) was treated with vehicle alone.

In vivo blockade of DC migration. BALB/c male mice aged 8–10 wk were sensitized by topical application of 3% (wt/vol) oxazolone in 95% aqueous ethanol to both ears (50 μl per ear). The next day, a further 50 μl of 3% (wt/vol) oxazolone was applied to the same site. On day 5, an

intraperitoneal injection of 0.5mg of antibody in PBS—6C7.1 (anti–VCAM-1) (48), YN1/1.7.4 (anti–ICAM-1) (47), or rat IgG—was administered. On day 6, the shaved abdomen was challenged by topical application of 0.8% oxazolone solution and 1.5mg/ml FITC at 150 μl per animal. 24 h after challenge, mice were killed, and the axillary and inguinal lymph nodes were removed. Tissue was disrupted by 0.5 mg/ml collagenase D (Roche) for 30 min at 37°C, passed through a 70-μm cell strainer (BD Biosciences), and stained with PE anti–mouse CD11c (BD Biosciences) for FACS analysis.

To observe blocking of DC migration from the dermis, contact hypersensitivity was induced by oxazolone in BALB/c male mice by application to the abdomen. 5 d after sensitization, either YN1/1.7.4 (anti–ICAM-1) or 0.5 mg rat IgG was administered by intraperitoneal injection. 24h later, oxazolone was applied to both ears. 8 h after the challenge, 10^6 CMFDA-labeled bone marrow–derived DCs per ear from a littermate (differentiated in vitro in 20 ng/ml IL-4 and GM-CSF) were dermally injected. 24 h later, animals were killed, and ear tissue was fixed in paraformaldehyde. Whole-mount staining was performed using hamster anti–mouse podoplanin with Alexa Fluor 568 and Cy5-conjugated goat anti–rat Cy5 to detect binding of neutralizing antibody within the tissue.

DNA microarray analyses. Total cellular RNA was isolated (RNeasy; QIAGEN) from freshly isolated primary HDLECs and MDLECs cultured for 24 h in EGM-2 MV medium alone or supplemented with 1 ng/ml TNF-α before synthesis and biotin labeling of cRNA probes and fragmentation according to standard Affymetrix protocols at the Cancer Research UK Microarray Facility (Paterson Institute for Cancer Research, Manchester, UK). Probes were hybridized for 16 h to Affymetrix GeneChip Human Genome U133 Plus 2.0 or Mouse 430 arrays, as appropriate, and processed using a GeneChip Fluidics Station 450 according to recommended protocols (EukGE-WS2v5; Affymetrix). Images were captured using the GeneChip Scanner 3000 (Affymetrix). Transcript levels were determined using GeneChip Operating Software (GCOS1.2; Affymetrix), and data were normalized by global scaling. Robust multi-array average (RMA) expression was measured by probe sequence information (GCRMA) in BioConductor R statistics and analyzed using Data Mining Tool (DMT 3.1; Affymetrix) and GeneSpring 7.2 (Silicon Genetics). Microarray data are available in the National Center for Biotechnology Information Gene Expression Omnibus (http://www.ncbi.nlm.nih.gov/geo/) under accession no. GSE6257.

MDDCs. PBMCs were obtained from healthy donors, and monocytes were purified by positive selection using anti-CD14–conjugated magnetic microbeads (Miltenyi Biotec). MDDCs were generated by culturing monocytes for 5 d in RPMI–10% FCS supplemented with 50 ng/ml GM-CSF and 10 ng/ml IL-4 (R&D Systems) and matured with LPS from 1μg/ml *Salmonella abortus* (Sigma-Aldrich). For fluorescent labeling, MDDCs were incubated with 2.5 μM Cell Tracker Green (Invitrogen) in EGM-2 MV media for 40 min, then washed in media and rested for 30 min.

MDDC-HDLEC transmigration assay. Primary HDLECs were seeded onto the underside of gelatin-coated Fluoroblok cell culture inserts (3-μm pore size; BD Biosciences) and incubated for 2 h at 37°C before being placed into a companion plate (BD Biosciences) containing EGM-2 MV medium. Cells were cultured until confluent and stimulated with 1 ng/ml TNF-α (R&D Systems) 24 h before use. To assess the contribution of individual adhesion molecules expressed in HDLECs, cells were incubated in the presence of blocking antibodies (see Antibodies) for 30 min before the addition of 0.5×10^6 fluorescently labeled MDDCs per well. To assess the contribution of ICAM-1 expressed on MDDCs, fluorescently labeled MDDCs were incubated at 37°C for 30 min in the presence of ICAM-1 blocking mAb 15.2 or mouse IgG and washed three times in medium before applying to the HDLEC monolayer. Numbers of MDDCs transmigrating through the filter and monolayer into the lower chamber were recorded at 30-min intervals on an automated fluorescent multiprobe plate reader (Synergy HT; Bio-Tek) at 37°C using KC[4] software (Biotech). The fluorescent signal was calibrated against a standard curve, and reverse transmigration was expressed as the number of DCs in the lower chamber.

To assess the permeability of the monolayer, 50 μg/ml Alexa Fluor 488 fluorescent dye was applied to the upper compartment of the Fluoroblok cell culture inserts with confluent HDLECs on the underside. Fluorescence in the lower chamber was recorded at 30-min intervals at 37°C, calibrated against a standard curve, and expressed as the concentration of dye in the lower chamber.

MDDC-HDLEC adhesion assay. Primary HDLECs were seeded in gelatin-coated 24-well dishes and cultured until confluent, then stimulated with 1 ng/ml TNF-α. Where appropriate, HDLECs were incubated in the presence of blocking antibodies (see Antibodies) for 30 min before the addition of fluorescently labeled 0.5×10^6 MDDCs per well. Plates were incubated for either 3 or 10 h, medium was removed, and cells were washed with PBS to remove nonadherent MDDCs. Numbers of MDDCs adhering were measured by a fluorescent plate reader, and the fluorescent signal was calibrated against a standard curve of fluorescently labeled DCs.

Online supplemental material. Detailed characterization of the effects of TNF-α on CAM expression by HDLECs and MDLECs (Figs. S1–S3), the association of DCs with ICAM-1–positive mouse lymphatics in vivo (Fig. S4), the phenotype of MDDCs (Fig. S5), and various features of the HDLEC in vitro transmigration assays (Figs. S6–S8) are available online. Tables S1 and S2 show Affymetrix GeneChip Human Genome U133 Plus 2.0 and Mouse 430 array data, respectively. Online supplemental material is available at http://www.jem.org/cgi/content/full/jem.20051759/DC1.

We thank Professor Nancy Hogg for providing ICAM-1 and LFA-1 blocking antibodies and Professor Dontscho Kerjaschki for the gift of primary HDLECs.

We acknowledge the financial support of the Medical Research Council and Cancer Research UK (project grant A3999).

The authors have no conflicting financial interests.

Submitted: 3 October 2005
Accepted: 26 October 2006

REFERENCES

1. Mellman, I., and R.M. Steinman. 2001. Dendritic cells: specialized and regulated antigen processing machines. *Cell*. 106:255–258.
2. Muller, W.A. 2003. Leukocyte-endothelial cell interactions in leukocyte transmigration and the inflammatory response. *Trends Immunol*. 24:327–334.
3. Randolph, G.J., V. Angeli, and M.A. Swartz. 2005. Dendritic cell trafficking to lymph nodes though lymphatic vessels. *Nat. Rev. Immunol*. 5:617–628.
4. Sallusto, F., P. Schaerli, P. Loetscher, C. Schaniel, D. Lenig, C.R. Mackay, S. Qin, and A. Lanzavecchia. 1998. Rapid and co-ordinated switch in chemokine receptor expression during dendritic cell maturation. *Eur. J. Immunol*. 28:2760–2769.
5. Saeki, H., A.M. Moore, M.J. Brown, and S.T. Hwang. 1999. Secondary lymphoid tissue chemokine (SLC) and CC chemokine receptor 7 (CCR7) participate in the emigration pathway of mature dendritic cells from the skin to regional lymph nodes. *J. Immunol*. 162:2472–2475.
6. Martin-Fontecha, A., S. Sebastiani, U.E. Hopken, M. Uggucioni, M. Lipp, A. Lanzavecchia, and F. Sallusto. 2003. Regulation of dendritic cell migration to the draining lymph node: impact on T lymphocyte traffic and priming. *J. Exp. Med*. 198:615–621.
7. Debes, G.F., C.N. Arnold, A.J. Young, S. Krautwald, M. Lipp, J.B. Hay, and E.C. Butcher. 2005. Chemokine receptor CCR7 required for T lymphocyte exit from peripheral tissues. *Nat. Immunol*. 6: 889–894.
8. Bromley, S., S.Y. Thomas, and A.D. Luster. 2005. Chemokine receptor CCR7 guides T cell exit from peripheral tissues and entry into afferent lymphatics. *Nat. Immunol*. 6:895–901.
9. Forster, R., A. Schubel, D. Breitfeld, E. Kremmer, I. Renner-Muller, E. Wolf, and M. Lipp. 1999. CCR7 co-ordinates the primary immune response by establishing functional microenvironments in secondary lymphoid organs. *Cell*. 99:23–33.

10. Gunn, M.D., S. Kyuwa, C. Tam, T. Kakiuchi, A. Matsuzawa, L.T. Williams, and H. Nakano. 1999. Mice lacking expression of secondary lymphoid organ chemokine have defects in lymphocyte homing and dendritic cell localization. *J. Exp. Med.* 189:451–460.
11. Luster, A.D., R. Alon, and U.H. von Andrian. 2005. Immune cell migration in inflammation: present and future therapeutic targets. *Nat. Immunol.* 6:1182–1190.
12. Sligh, J.E., C.M. Ballantyne, S.S. Rich, H.K. Hawkins, C.W. Smith, A. Bradley, and A.L. Beaudet. 1993. Inflammatory and immune responses are impaired in mice deficient in intercellular adhesion molecule 1. *Proc. Natl. Acad. Sci. USA.* 90:8529–8533.
13. Xu, H., H. Guan, G. Zu, D. Bullard, J. Hanson, M. Slater, and C.A. Elmets. 2001. The role of ICAM-1 molecule in the migration of Langerhans cells in the skin and regional lymph node. *Eur. J. Immunol.* 31:3085–3093.
14. Young, A.J., T.J. Seabrook, W.L. Marston, L. Dudler, and J.B. Hay. 2000. A role for lymphatic endothelium in the sequestration of recirculating gamma delta T cells in TNF-alpha-stimulated lymph nodes. *Eur. J. Immunol.* 30:327–334.
15. Skobe, M., and M. Detmar. 2000. Structure, function, and molecular control of the skin lymphatic system. *J. Investig. Dermatol. Symp. Proc.* 5:14–19.
16. Oliver, G., and M. Detmar. 2002. The rediscovery of the lymphatic system: old and new insights into the development and biological function of the lymphatic vasculature. *Genes Dev.* 16:773–783.
17. Leak, L.V. 1970. Electron microscopic observations on lymphatic capillaries and the structural components of the connective tissue-lymph interface. *Microvasc. Res.* 2:361–391.
18. Leak, L.V. 1976. The structure of lymphatic capillaries in lymph formation. *Fed. Proc.* 35:1863–1871.
19. Witte, M.H., K. Jones, J. Wilting, M. Dictor, M. Selg, N. McHale, J.E. Gershenwald, and D.G. Jackson. 2006. Structure function relationships in the lymphatic system and implications for cancer biology. *Cancer Metastasis Rev.* 25:159–184.
20. Barreiro, O., M. Yanez-Mo, J.M. Serrador, M.C. Montoya, M. Vicente-Manzanares, R. Tejedor, H. Furthmayr, and F. Sanchez-Madrid. 2002. Dynamic interaction of VCAM-1 and ICAM-1 with moesin and ezrin in a novel endothelial docking structure for adherent leukocytes. *J. Cell Biol.* 157:1233–1245.
21. Carman, C.V., and T.A. Springer. 2004. A transmigratory cup in leukocyte dispedesis both through individual vascular endothelial cells and between them. *J. Cell Biol.* 167:377–388.
22. Stoitzner, P., K. Pfaller, H. Stossel, and N. Romani. 2002. A close-up view of migrating Langerhans cells in the skin. *J. Invest. Dermatol.* 118:117–125.
23. Stoitzner, P., S. Holzmann, A.D. McLellan, L. Ivarsson, H. Stossel, M. Kapp, U. Kammerer, P. Douillard, E. Kampgen, F. Koch, et al. 2003. Visualization and characterization of migratory Langerhans cells in murine skin and lymph nodes by antibodies against Langerin/CD207. *J. Invest. Dermatol.* 120:266–274.
24. Banerji, S., A.J. Day, J.D. Kahmann, and D.G. Jackson. 1998. Characterization of a functional hyaluronan-binding domain from the human CD44 molecule expressed in *Escherichia coli*. *Protein Expr. Purif.* 14:371–381.
25. Prevo, R., S. Banerji, D.J. Ferguson, S. Clasper, and D.G. Jackson. 2001. Mouse LYVE-1 is an endocytic receptor for hyaluronan in lymphatic endothelium. *J. Biol. Chem.* 276:19420–19430.
26. Jackson, D.G. 2004. Biology of the lymphatic marker LYVE-1 and applications in research into lymphatic trafficking and lymphangiogenesis. *APMIS.* 112:526–538.
27. Breiteneder-Geleff, S., A. Soleiman, H. Kowalski, R. Horvat, G. Amann, E. Kriehuber, K. Diem, W. Weninger, E. Tschachler, K. Alitalo, and D. Kerjaschki. 1999. Angiosarcomas express mixed endothelial phenotypes of blood and lymphatic capillaries: podoplanin as a specific marker for lymphatic endothelium. *Am. J. Pathol.* 154:385–394.
28. Wigle, J.T., and G. Oliver. 1999. Prox-1 function is required for the development of the murine lymphatic system. *Cell.* 98:769–778.
29. Wigle, J.T., N. Harvey, M. Detmar, I. Lagutina, G. Grosveld, M.D. Gunn, D.G. Jackson, and G. Oliver. 2002. An essential role for Prox1 in the induction of the lymphatic endothelial cell phenotype. *EMBO J.* 21:1505–1513.
30. Muller, W.A., C.M. Ratti, S.L. McDonnell, and Z.A. Cohn. 1989. A human endothelial cell–restricted, externally disposed plasmalemmal protein enriched in intercellular junctions. *J. Exp. Med.* 170:399–414.
31. Rubbia-Brandt, L., B. Terris, E. Giostra, B. Dousset, P. Morel, and M.S. Pepper. 2004. Lymphatic vessel density and vascular endothelial growth factor-C expression correlate with malignant behavior in human pancreatic endocrine tumors. *Clin. Cancer Res.* 10:6919–6928.
32. Makinen, T., T. Veikkola, S. Mustjoki, T. Karpanen, B. Catimel, E.C. Nice, L. Wise, A. Mercer, H. Kowalski, D. Kerjaschki, et al. 2001. Isolated lymphatic endothelial cells transduce growth, survival and migratory signals via the VEGF-C/D receptor VEGFR-3. *EMBO J.* 20:4762–4773.
33. Podgrabinska, S., P. Braun, P. Velasco, B. Kloos, L. Janes, M.S. Pepper, D.G. Jackson, and M. Skobe. 2002. Molecular characterization of lymphatic endothelial cells. *Proc. Natl. Acad. Sci. USA.* In press.
34. Hirakawa, S., Y.K. Hong, N. Harvey, V. Schacht, K. Matsuda, T. Libermann, and M. Detmar. 2003. Identification of vascular lineage-specific genes by transcriptional profiling of isolated blood vascular and lymphatic endothelial cells. *Am. J. Pathol.* 162:575–586.
35. Nisato, R.E., J.A. Harrison, R. Buser, L. Orci, C. Rinsch, R. Montesano, P. Dupraz, and M.S. Pepper. 2004. Generation and characterization of telomerase-transfected human lymphatic endothelial cells with an extended life span. *Am. J. Pathol.* 165:11–24.
36. Schlingemann, R.O., G.M. Dingjan, J.J. Emeis, J. Blok, S.O. Warnaar, and D.J. Ruiter. 1985. Monoclonal antibody PAL-E specific for endothelium. *Lab. Invest.* 52:71–76.
37. Niemela, H., K. Elima, T. Henttinen, H. Irjala, M. Salmi, and S. Jalkanen. 2005. Molecular identification of pal-E, a widely used endothelial-cell marker. *Blood.* 106:3405–3409.
38. Pober, J.S., M.P. Bevilacqua, D.L. Mendrick, L.A. Lapierre, W. Fiers, and M.A. Gimbrone. 1986. Two distinct monokines, interleukin 1 and tumor necrosis factor, each independently induce the biosynthesis and transient expression of the same antigen on the surface of cultured human vascular endothelial cells. *J. Immunol.* 136:1680–1687.
39. Dustin, M.L., and T.A. Springer. 1988. Lymphocyte function-associated antigen 1 (LFA-1) interaction with intercellular adhesion molecule 1 (ICAM-1) is one of at least three mechanisms for lymphocyte adhesion to cultured endothelial cells. *J. Cell Biol.* 107:321–331.
40. Carlos, T.M., B.R. Schwarz, N.L. Kovach, E. Yee, M. Rosa, L. Osborn, G. Chi-Rosso, B. Newman, R. Lobb, and J.M. Harlan. 1990. Vascular cell adhesion molecule-1 mediates lymphocyte adherence to cytokine-activated cultured human endothelial cells. *Blood.* 76:965–970.
41. Mackay, F., H. Loetscher, D. Stueber, G. Gehr, and W. Lesslauer. 1993. Tumor necrosis factor α (TNF-α)–induced cell adhesion to human endothelial cells is under dominant control of one TNF receptor type, TNF-R55. *J. Exp. Med.* 177:1277–1286.
42. Muller, W.A., and S. Weigl. 1992. Monocyte-selective transendothelial migration: dissection of the binding and transmigration phases by an in vitro assay. *J. Exp. Med.* 176:819–828.
43. Kriehuber, E., S. Breiteneder-Geleff, M. Groeger, A. Soleiman, S.F. Schoppmann, G. Stingl, D. Kerjaschki, and D. Maurer. 2001. Isolation and characterization of dermal lymphatic and blood endothelial cells reveal stable and functionally specialized cell lineages. *J. Exp. Med.* 194:797–808.
44. Homey, B., H. Alenius, A. Muller, H. Soto, E.P. Bowman, W. Yuan, L. McEvoy, A.I. Lauerma, T. Assmann, E. Bunemann, et al. 2002. CCL27-CCR10 interactions regulate T cell-mediated skin inflammation. *Nat. Med.* 8:157–165.
45. Grabbe, S., and T. Schwarz. 1998. Immunoregulatory mechanisms involved in elicitation of allergic contact hypersensitivity. *Immunol. Today.* 19:37–44.
46. Cumberbatch, M., R.J. Dearman, C.E. Griffiths, and I. Kimber. 2003. Epidermal Langerhans cell migration and sensitisation to chemical allergens. *APMIS.* 111:797–804.
47. Takei, F. 1985. Inhibition of mixed lymphocyte response by a rat monoclonal antibody to a novel murine lymphocyte activation antigen (MALA-2). *J. Immunol.* 134:1403–1407.

48. Engelhardt, B., M. Laschinger, M. Schulz, U. Samulowitz, D. Vestweber, and G. Hoch. 1998. The development of experimental autoimmune encephalomyelitis in the mouse requires α4β1-integrin but not α4β7-integrin. *J. Clin. Invest.* 102:2096–2105.
49. Weinlich, G., M. Heine, and H. Stossel. 1998. Entry into afferent lymphatics and maturation in situ of migrating cutaneous dendritic cells. *J. Invest. Dermatol.* 110:441–448.
50. Butcher, E.C. 1991. Leukocyte-endothelial cell recognition: three (or more) steps to specificity and diversity. *Cell.* 67:1033–1036.
51. Schenkel, A.R., Z. Mamdouh, and W.A. Muller. 2004. Locomotion of monocytes on endothelium is a critical step during extravasation. *Nat. Immunol.* 5:393–400.
52. Johnson-Leger, C., M. Aurrand-Lions, and B.A. Imhof. 2000. The parting of the endothelium: miracle, or simply a junctional affair? *J. Cell Sci.* 113:921–933.
53. Luscinskas, F.W., S. Ma, A. Nusrat, C.A. Parkos, and S.K. Shaw. 2002. Leukocyte transendothelial migration: a junctional affair. *Semin. Immunol.* 14:105–113.
54. Schenkel, A.R., Z. Mamdouh, X. Chen, R.M. Liebman, and W.A. Muller. 2002. CD99 plays a major role in the migration of monocytes through endothelial junctions. *Nat. Immunol.* 3:143–150.
55. Cera, M.R., A. Del Prete, A. Vecchi, M. Corada, I. Martin-Padura, T. Motoike, P. Tonetti, G. Bazzoni, W. Vermi, F. Gentili, et al. 2004. Increased DC trafficking to lymph nodes and contact hypersensitivity in junctional adhesion molecule-A-deficient mice. *J. Clin. Invest.* 114:729–738.
56. Millan, J., L. Hewlett, M. Glyn, D. Toomre, P. Clark, and A. Ridley. 2006. Lymphocyte transcellular migration occurs through recruitment of endothelial ICAM-1 to caveola- and F-actin-rich domains. *Nat. Cell Biol.* 8:113–123.
57. Dieu, M.C., B. Vanbervliet, A. Vicari, J.M. Bridon, E. Oldham, S. Ait-Yahia, F. Briere, A. Zlotnik, S. Lebecque, and C. Caux. 1998. Selective recruitment of immature and mature dendritic cells by distinct chemokines expressed in different anatomic sites. *J. Exp. Med.* 188:373–386.
58. von Andrian, U.H., and T.R. Mempel. 2003. Homing and cellular traffic in lymph nodes. *Nat. Rev. Immunol.* 3:867–878.
59. Middleton, J., A.M. Patterson, L. Gardner, C. Schmutz, and B.A. Ashton. 2002. Leukocyte extravasation: chemokine transport and presentation by the endothelium. *Blood.* 100:3853–3860.
60. Palframan, R.T., S. Jung, G. Cheng, W. Weninger, Y. Luo, M. Dorf, D.R. Littman, B.J. Rollins, H. Zweerink, A. Rot, and U.H. von Andrian. 2001. Inflammatory chemokine transport and presentation in HEV: a remote control mechanism for monocyte recruitment to lymph nodes in inflamed tissues. *J. Exp. Med.* 194:1361–1373.
61. Banerji, S., J. Ni, S.X. Wang, S. Clasper, J. Su, R. Tammi, M. Jones, and D.G. Jackson. 1999. LYVE-1, a new homologue of the CD44 glycoprotein, is a lymph-specific receptor for hyaluronan. *J. Cell Biol.* 144:789–801.
62. Dittel, B.N., E.A. Wayner, J.B. McCarthy, and T.W. LeBien. 1993. Regulation of human B cell precursor adhesion to bone marrow stromal cells by cytokines which exert opposing effects on the expression of vascular cell adhesion molecule-1(VCAM-1). *Blood.* 81:2272–2282.
63. Carmichael, J., W.G. DeGraff, A.F. Gazdar, J.D. Minna, and J.B. Mitchell. 1987. Evaluation of a tetrazolium-based semiautomated colorimetric assay: assessment of chemosensitivity testing. *Cancer Res.* 47:936–942.